ECE 513 Project Report

Ufuk Soylu(usoylu2)

February 8, 2021

1 Introduction

In active array imaging, a transmitter emits an excitation signal and then forms an image using reflections collected at an array of sensors.[1]. This imaging technique has found many applications from medicine to security. One of the medical imaging technique that uses this idea is ultrasound imaging.

Ultrasound which is a type of sound energy that is over hearing range(over 20.000Hz). In ultrasound imaging, an array of piezoelectric sensors is used to transmit ultrasound waves to human body and scattered waves collected at the same array of sensors. Based on collected scattering waves, medical image is generally formed by using beam forming which is a linear combination of measurement of each sensor.

Early beginnings of ultrasound imaging can be traced back to Sonar and Radar imaging. After World War I and II, Sonar and Radar imaging technology was ready to use in biomedical context. Subsequently, medical ultrasound imaging was commercialized in early 1950s in Japan, the United States, and Sweden. From that time, ultrasound imaging area have been a very active area for researchers due to advantages of ultrasound imaging in comparison to other biomedical imaging modalities [2].

There are mainly four reasons that make ultrasound imaging attractive to researchers and medical society. The first reason is that ultrasound energy is very safe. American Institute of Ultrasound Medicine(AIUM) states that *"... **no confirmed biological effects** on patients or instrument operators caused by exposure at intensities typical of present diagnostic ultrasound instruments have ever been reported. Although the possibility exists that such biological effects may be identified in the future, current data indicate that the benefits to patients of the prudent use of diagnostic ultrasound outweigh the risks, if any, that may be present ..." [3]* . The second reason that makes ultrasound attractive is that ultrasound imaging systems are inexpensive. When it is compared to other common medical modalities such as MRI and CT, it does not require any facility. Therefore, medical ultrasound imaging is the second most used imaging systems among all medical imaging systems [2] and it is very crucial for developing and undeveloped countries due to its low cost. The third reason that makes ultrasound attractive is that it has high frame rates. State-of-art ultrasound imaging systems can go up to 1000 frames per second which allows medical examiner to examine very fast moving objects such as hearth valves in real time. Being able to examine in real time provides medical examiner critical medical information. The last reason that makes ultrasound attractive is that it is portable. If a patient is confined to bed, ultrasound imaging is the best option due to its portability. Recently, handheld ultrasound devices becoming available for medical ultrasound imaging which can significantly revolutionize medical imaging by decreasing the cost and increasing the portability [4].

The ultimate goal of this project is to decrease the cost of medical ultrasound imaging systems so that they can become common household items such as medical thermometers or blood pressure cuffs. Subsequently, everyone can do medical imaging at their home when it is necessary. In other words, the main goal is to increase the affordability of medical imaging systems so that everyone can have it at their home.

In this work, the cost and portability of medical system will be tried to improved by decreasing the required number of sensors. When sensor array imaging systems need to be used in low-cost commercial applications, it is desirable to reduce the number of elements in an array and use smarter algorithms to reduce the cost of the system. Therefore, main motivation is to decrease number of sensors element without losing image quality. Organization of the paper is as follows: 1) Introduction, 2) The Primary Paper, 3) Mistakes in the Paper, 4) Simulation Results, 5) Conclusion. In Introduction part, the question "Why?" is answered by providing the goal and main motivation. In The Primary Paper part, the question "What?" is answered by providing the main intuitions of the paper and the question "How?" is answered by providing rigorous arguments and justifications of their method. Additionally, in this part, the connections between

the paper and course content is established. Missing steps in the arguments are filled-in by using ECE 513 course content. In third part which is Mistakes in the Paper, mistakes are stated and corrected. These mistakes are generally minor mistakes such as misuse of terminology or some notation mistakes. In the Simulation Results part, Field 2 which is a program for simulating realistic bio-medical ultrasound imaging settings, is used to test the paper idea in the context of ultrasound imaging. Additionally, two quantitative measures namely MSE and SSIM are used to compare results. In the last part which is Conclusion part, observations from results are discussed.

2 The Primary Paper

The name of the primary paper is "Trading Beams for Bandwidth: Imaging with Randomized Beam-forming". In the paper, they studied actively imaging a range-limited far-field scene using an antenna array with broadband measurements[1]. They introduce a novel trade-off between the number of spatial array measurements and range-limit. Their main observation is that broadband measurements of a range-limited targets under far-field assumption lie in a lower dimensional subspace. Therefore, they take advantage of this fact and reconstruct range-limited targets by using spatially under-sampled array data without losing image quality [1]. Additionally, they also provide theoretical justification for proposed signal acquisition method by using matrix sketching methods [5]. Hence, they showed that traditional beam-forming is wasteful when the target scene is range-limited. Subsequently, their proposed algorithm is desirable to be used in low-cost applications since required number of sensor is less than traditional methods. Main key points can be summarized as follows:

- Main intuition is that signals which are concentrated maximally in a given time interval and a frequency interval are well-approximated using a subspace of dimension approximately equal to the product of the lengths of the intervals.
- They extend the main intuition to array imaging context by adding range-limited assumption on target scene. By its nature, array imaging measurements are band-limited due to finite aperture size. When we add range-limit on target scene, the main intuition suggests that measurements lie on a lower dimensional subspace.
- Subsequently, their main observation is that a set of spatial, broadband measurements of such range-limited targets have a limited degree of freedom. Therefore, this fact can be used to under sample sensor array.
- Their work can be evaluated as compressed sensing but there is an important distinction. The compressed sensing paradigm generally imposes the target scene to be sparse. In their work, they do not impose any form of sparsity. Instead, they imposes range limitedness on target scene.
- Therefore , they introduce a novel trade off for compressed sensing paradigm: range-limit and number of sensors.
- They provide theoretical justification by using matrix sketching which is a set of dimensionality reduction techniques used in linear algebra community. However, their theoretical justification is not for random binary matrix which they propose to use to under sample the sensor array. Their theoretical justification is for random Gaussian matrix and they do simulations to show that it is valid for random binary matrix.
- The paper examines broadband excitation under far filed assumption for range limited target scenes. So, it has three assumptions: broadband source, far field and range limited target scenes. Broadband excitation is somehow valid for ultrasound imaging since source signal has to be time limited. Range limited target scene is also valid for ultrasound imaging since human body, which is range limited, is the target scene.
- The proposed method's major caveat for ultrasound imaging is far field assumption. In ultrasound imaging, strong far field assumptions are generally not valid. However, in the paper the assumption can be considered as intermediate assumption. Therefore, this assumption is a reasonable assumption.

2.1 Main Intuition

The main intuition is that signals which are concentrated maximally in a given given time interval and a frequency interval are well-approximated using a subspace of dimension approximately equal to the product of the lengths of the intervals [6],[7]. This idea is well studied for one dimensional signals and two dimensional signals. The intuition can be also examined by considering time or band limited signals and Fourier series expression as follows:

Let $f(x)$ be a periodic function with period L. Then it can be expressed by using complex exponential.

$$f(x) = \sum_{n=-\infty}^{\infty} A_n e^{i(2\pi nx/L)}$$

In order to the intuition holds, $f(x)$'s energy should be concentrated maximally in a time interval and a frequency interval. Let's consider the band limited part firstly. We can assume that bandwidth of $f(x)$ is between $(-f_0, f_0)$. Then $f(x)$ can be expressed as follows:

$$f(x) = \sum_{n=-Lf_0}^{Lf_0} A_n e^{i(2\pi nx/L)}$$

Subsequently, we can make some observations:

- Complex exponential signals $e^{i(2\pi nx/L)}$ form a basis for band limited signals $f(x)$.
- Number of basis elements is $2Lf_0$. That is equal to bandwidth interval $\times$ time period.

In order to be more rigorous, we can only take one period of $f(x)$ by multiplying it with a rect function. Then it becomes time limited signals. For this case, Fourier series coefficients will be convolved with sinc function. However, most of the energy will be concentrated in a frequency interval. So we can represent such functions very well by using $2Lf_0$ complex exponential. Therefore, we can conclude that such functions have a finite degree of freedoms which is a consequence of simultaneous concentration of energy in both time and frequency domains.

The extension of the intuition from one dimensional signals to two dimensional signals such as images is straightforward. If two dimensional signals' energies are simultaneously concentrated in both spatial and spectral domains then those signals can be approximated very well by using a number of basis functions that is proportional to the product of the area/volume of the spatial and spectral supports. This has been studied well [6]. An efficient basis for the representation of such signals is the prolate basis[6].

This idea is applied by introducing range limited assumption on target scene. Range limited assumption guarantees that the sensor array measurements are concentrated in spatial domain. On the other hand, finite aperture and finite bandwidth guarantee that the sensor array measurements are concentrated in spectral domain. Subsequently, their main observation is that a set of spatial, broadband measurements of such range-limited targets lie in a lower dimensional subspace and hence have a limited number of degrees of freedom. By taking advantage of this fact, the paper proposes that under-sampled array data yield reconstructions as good as those obtained with conventional sensor array imaging.

2.2 Active Array Imaging

In this section, it will be emphasized that broadband array measurements provide a set of band limited Fourier domain samples of the target scene. the imaging setup is given in Figure 1.

Imaging scene is equivalent to reflectivity map $p(r, \theta)$. The sensor array is located between $\frac{-D}{2}$ and $\frac{D}{2}$. The system consists of only one transmitting element which is co-located with the receiver at array center. Let's denote excitation signal as $s(t)$.

We can first examine the narrow-band excitation, i.e. $s(t) = e^{i2\pi ct/\lambda}$. Then received signal at position d is as follows:

$$\widetilde{y}_{d,\lambda}(t) = \mathrm{e}^{\mathrm{j}2\pi ct/\lambda} \int_{-\pi/2}^{\pi/2} \int p(r,\theta) \mathrm{e}^{-\mathrm{j}2\pi(2r - d\sin\theta)/\lambda} dr d\theta$$

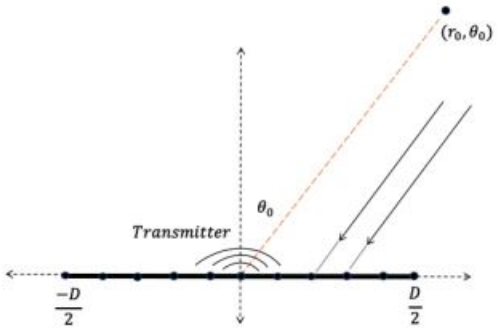

Figure 1: Imaging Setup

Generally, complex envelope of such signals is used due to many advantages. So, complex envelope is as follows:

$$y_{d,\lambda} = \int_{-\pi/2}^{\pi/2} \int p(r,\theta) \mathrm{e}^{-\mathrm{j}2\pi(2r - d\sin\theta)/\lambda} dr d\theta = \widehat{x}_c\left(\omega_r, \omega_\tau\right)$$

where $\widehat{x}_c$ denotes the Fourier transform of $x_c(r,\tau) = \frac{p(r, sin^{-1}(2\tau))}{\sqrt{1-4\tau^2}}$, $w_r = \frac{2}{\lambda}$,$w_\tau = \frac{-2d}{\lambda}$ and $\tau = \frac{sin(\theta)}{2}$. This shows that the antenna aperture measures the Fourier transform of x_c which is a warped version of the target scene.

If the excitation signal is broadband then received signal at location d is as follows:

$$\widetilde{y}_d(t) = \int_{-\pi/2}^{\pi/2} \int p(r,\theta) s_b(t - r/c - d\sin\theta) dr d\theta$$

Now, it is clear that a finite aperture and a finite bandwidth excitation signal offer band limited measurements which can be seen in Figure 2. When we have discrete sensor array, we only collect discrete samples in the Fourier domain which can be seen in Figure 3

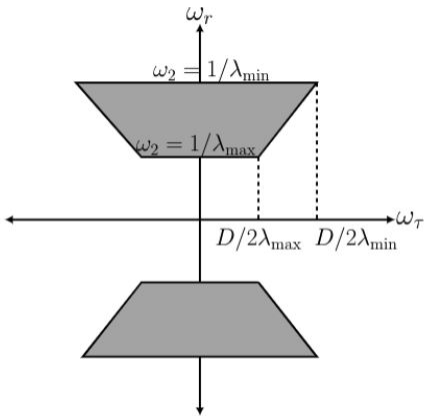

Figure 2: The region in the Fourier Domain of a target scene acquired by using broadband excitation

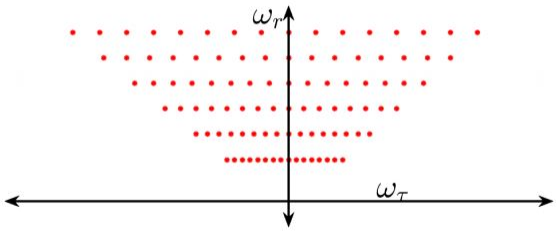

Figure 3: With a discrete array, we can only collect discrete samples in the Fourier Domain

2.3 Signal Model

In this section, the forward model will be introduced based on conventional imaging scheme. Then coded aperture measurements will be introduced.

Let the linear sensor array has M discrete sensor elements placed uniformly at coordinates $d_{\frac{-M}{2}}, \cdots, d_{\frac{M}{2}} \in [-D/2, D/2]$. Additionally, let's consider discrete set of K excitation wavelengths $\{\lambda_1 = \lambda_{\min}, \lambda_2, \cdots, \lambda_K = \lambda_{\max}\}$.

Then set of all measurements can be denoted vector $y \in \mathbb{C}^{MK}$ to represent $\{y_{m,\lambda}\}$ where $m = 1, \ldots, M$ and $\lambda \in \{\lambda_1, \ldots, \lambda_K\}$. Let's assume that target scene with delta thickness at range R_0. Receive signal at mth sensor and for specific λ is as follows:

$$\widetilde{y}_{m,\lambda}(t) = \mathrm{e}^{\mathrm{j}2\pi(ct+R_0)/\lambda} \int_{-1/2}^{1/2} p\left(R_0, \tau\right) \mathrm{e}^{-\mathrm{j}2\pi\omega_\tau \tau} \mathrm{d}\tau$$

For computational purposes, we can discretize the target scene and the imaging operator. Let's denote $x_{R_0} \in \mathbb{R}^N$ where $N > M$. Similarly, integral mapping the target scene to the array measurements at wavelength λ can be discretized as a matrix since it is a linear operator as matrix $A_{R_{0,\lambda}} \in \mathbb{C}^{M \times N}$ operating on x_{R_0}:

$$A_{R_0,\lambda}(m,n) = \exp^{-j2\pi R_0/\lambda} \exp^{-i2\pi 2d_m(-0.5+n/N)/\lambda}$$

For more general case, let's consider target scene with a range limit R. Then target scene can be denoted as $x_R \in \mathbb{R}^{\mathbb{ND}}$ where D represents samples along radial dimension. Then operator can be discretized as follows:

$$A_{R,\lambda}(m,n) = \exp^{-j2\pi(2d_m(-0.5+n_\tau/N)+(R_{\min}+d_r R/D))/\lambda}$$

where $d_r = \lfloor n/N + 1 \rfloor$, $n_\tau = mod(n, N)$ and $A_{R,\lambda} \in \mathbb{C}^{M \times ND}$.

$$\implies y_{R,\lambda} = A_{R,\lambda} x_R$$

We can drop subscript R for simplicity and all measurements can be expressed as follows:

$$y = \begin{bmatrix} y_{\lambda_1} \\ y_{\lambda_2} \\ \vdots \\ y_{\lambda_K} \end{bmatrix} = \begin{bmatrix} A_{\lambda_1} \\ A_{\lambda_2} \\ \vdots \\ A_{\lambda_K} \end{bmatrix} x_0 = Ax_0 \tag{1}$$

The measurements lie in the column space of A. the effective dimension of this subspace determines the number of degrees of freedom in y. Measurements can be collected with a coded aperture which refers to collecting linear combinations of the array outputs. We can model the measurements as follows:

$$z = \Phi y = \begin{bmatrix} \phi & 0 & \cdots & 0 \\ 0 & \phi & \cdots & 0 \\ \vdots & \vdots & \ddots & \vdots \\ 0 & 0 & \cdots & \phi \end{bmatrix} \begin{bmatrix} y_{\lambda_1} \\ y_{\lambda_2} \\ \vdots \\ y_{\lambda_K} \end{bmatrix} = \Phi A x_0 \tag{2}$$

The main goal of the paper is to show that the target scene can be constructed using highly underdetermined matrices $\phi \in \mathbb{R}^{l \times M}$ with no loss compared to the reconstruction with full set of measurements y.

2.4 Coded Aperture Image Reconstruction

Image reconstruction method for aperture coded measurement model is to solve ordinary least squares problem:

$$\arg\min_x \|\Phi y - \Phi A x\|_2^2 \quad where \quad \Phi = \begin{bmatrix} \phi & 0 & \cdots & 0 \\ 0 & \phi & \cdots & 0 \\ \vdots & \vdots & \ddots & \vdots \\ 0 & 0 & \cdots & \phi \end{bmatrix} \tag{3}$$

On the other hand, ordinary least squares solution to full data is as follows:

$$\arg\min_x \|y - Ax\|_2^2 \tag{4}$$

The question to be answered is that what is the sample complexity l that can achieve the same reconstruction result as equation 4 by using equation 3. Problems in 3 are the subject of matrix sketching [5]. The new matrix has much smaller dimensions that ambient dimension and is used to solve original linear algebra problem. So the solution can be computed cheaply in terms of computation complexity.

2.5 Signal Recovery from Aperture Coded Measurements

In this section, mathematical guarantees will be explained for skecthed problem described in equation 3 for particular Φ structure. We will state the conditions for 3 and 4 having the same solution. Solution for 4 is as follows:

$$x_{MNLS} = A^{\dagger}y = A^{\dagger}Ax_0 = VV^{\star}x_0$$

where $A = U\Sigma V^{\star}$ is the SVD decomposition and $A^{\dagger}$ is the pseudo-inverse of A. From [8] Theorem 1.15, projector operator on range of V can be defined as $P_{R(V)} = VV^{\star}$ when V is orthonormal matrix. Additionally, form [8] Thm 2.4, we know that $R(A^{\star}) = R(V)$. Subsequently, solution of 4 is as follows:

$$x_{MNLS} = VV^{\star}x_0 = P_{R(V)}x_0 = P_{R(A^{\star})}x_0$$

Similary, solution of the 3 is as follows:

$$x_{M\hat{N}LS} = (\Phi A)^{\dagger}\Phi y = (\Phi A)^{\dagger}(\Phi A)x_0 = V_{(\Phi A)}V^{\star}_{(\Phi A)}x_0 = P_{R(V_{(\Phi A)})}x_0 = P_{R((\Phi A)^{\star})}x_0$$

Subsequently, we can conclude that any operator Φ that preserves the row space of A will give the true solution. Then the condition is as follows:

$$P_{R((\Phi A)^{\star})}x_0 - P_{R(A^{\star})}x_0 = 0, \forall x_0 \iff P_{R(A^{\star})} - P_{R((\Phi A)^{\star})} = 0 \iff (P_{R(A^{\star})} - P_{R((\Phi A)^{\star})})A^{\star} = 0$$

Therefore, for any sketching matrix Φ a necessary and sufficient condition is $||(I - P_{R((\Phi A)^{\star})})A^{\star}|| = 0$.

Let's define $\text{rank}(A) = r \ll \min(m, n) \quad where \quad A \in \mathbb{C}^{m\times n}$. In matrix sketching literature, it has been well established that if Φ is a $l \times m$ dense standard normal random matrix with $l \geq r$ then the necessary and sufficient condition holds. In our problem, Φ has a special structure namely repeated block diagonal (RBD) matrix. The paper provides three theorems for RBD matrix case. Theorem 6.1 provides a simple but non-trivial estimate for l. Then, theorem 6.2 and 6.3 improves this result. For curious readers, the proofs can be found in the original paper. The proofs are based on genericity argument.

THEOREM 6.1. *For a given matrix A of size $Km \times n$, let the d_i be defined as follows:*

$$\begin{bmatrix} A_1 \\ A_2 \\ . \\ A_k \end{bmatrix} = \begin{bmatrix} C_{11} & 0 & \cdots & 0 \\ C_{21} & C_{22} & \cdots & 0 \\ \vdots & \vdots & \ddots & \vdots \\ C_{k1} & C_{k2} & \cdots & C_{kk} \end{bmatrix} \begin{bmatrix} V_1^T \\ V_2^T \\ \vdots \\ V_k^T \end{bmatrix} = CV^T$$

The above decomposition is called as block QR factorization of A where $C_{ij} \in \mathbb{R}^{m\times d_j}$. Let Φ be a block diagonal matrix with repeated diagonal block ϕ of size $l \times m$ and whose entries are chosen i.i.d. from the standard normal distribution. Define $d_0 = max_i d_i$. For $l \geq d_0$, $||(I - P_{R((\Phi A)^{\star})})A^{\star}|| = 0$ with prob 1.

THEOREM 6.2. *Let $A = \begin{bmatrix} A_1 \\ A_2 \end{bmatrix}$, with $\text{row}(A_1) \subseteq \text{row}(A_2)$. Assume A_2 is full row rank and define $U = A_1A_2^T$. If the entries of ϕ are drawn from a continuous distribution, with probability 1, $\Phi A = \begin{bmatrix} \phi A_1 \\ \phi A_2 \end{bmatrix}$ is full row rank for any $l \leq n/2$ if and only if no real eigenvalue of U has an algebraic multiplicity greater than $n/2$. Consequently, for $l \geq n/2$, $\left\|\left(I - P_{(\Phi A)^{\star}}\right)A^T = 0\right\|$ with probability 1.*

THEOREM 6.3. *Given an ensemble of K matrices $\{A_i\}$ for $i = 1\ldots, K$, each of size $m \times n$ and a matrix $\phi \in \mathbb{R}^{l\times m}$ with entries drawn from the standard normal distribution, $\Phi A = \begin{bmatrix} \phi A_1 \\ \ldots \\ \phi A_K \end{bmatrix}$ is full row rank if there exists an orthonormal basis $V_S \in \mathbb{R}^{l\times m}$ such that the $kl \times n$ size matrix $\widehat{M} = \begin{bmatrix} V_S A_1 \\ \vdots \\ V_S A_K \end{bmatrix}$ has full row rank. Consequently, for $l = r/K$, $\left\|\left(I - P_{(\Phi A)^{\star}}\right)A^T = 0\right\|$ with probability 1.*

3 Mistakes in Paper

The paper is a very recent paper which was published on 31 January 2019. It is on arxiv. There are minor mistakes that I have realized. They are mostly misuse of terminology or minor calculation mistakes. However, mistakes do not affect the main idea and proposed method is still valid.

First mistake is from 3.1. Propagation Model and Fourier Domain Samples. They state that for an excitation signal $s(t)$, signal received at the array location d is $s(t - r_0/c - dsin(\theta)/c)$. However this information is wrong. When we do far field assumption, what we get is $s(t-2r_0/c+dsin(\theta)/c)$. Subsequently, analysis in part 3 is not completely true. Variables should be updated with correct scalar in order to compensate this mistake. For instance $w_r = \frac{2}{\lambda}$ and $w_\tau = \frac{-2d}{\lambda}$.

Second mistake or misuse of terminology is from again 3.1 Propagation Model and Fourier Domain Samples. While deriving that measurements are Fourier Domain samples of target scene, they take complex envelope of measurements. However, they say complex amplitude instead of complex envelope which was confusing.

Third mistake or misuse of terminology is from 9. Signal recovery from aperture coded measurements. For problem 4, they state that

$$x_{\text{LS}} = A^\dagger y$$

However, since A is low dimensional matrix, they are not only getting least square solution. When we multiply the measurement with pseudo inverse of such a matrix, we get minimum norm least squares solution. So, the following representation would be more clear:

$$x_{\text{MNLS}} = A^\dagger y$$

4 Simulation Results

The method proposed by the paper is tested for medical ultrasound imaging. Realistic simulations are done by using program Field II. Field II is a program for simulating ultrasound transducer fields and ultrasound imaging using linear acoustics. The program uses the Tupholme-Stepanishen method for calculating the emitted and pulse-echo fields for both the pulsed and continuous wave case for a large number of different transducers. Also any kind of linear imaging can be simulated as well as realistic images of human tissue [9],[10]. The program is running under Matlab and Matlab code for the simulations is provided in Appendix.

There are four different simulation scenarios. For all cases kerf, which is the distance between ultrasound elements, is chosen as 0.03 mm and width which is the width of each ultrasound sensor is chosen as 0.27 mm. For narrow-band excitation, the excitation signal consists of only one frequency:5MHz. The excitation signal is obtained by applying Hann windowing. For all cases, target scene consists of 16 point scatters which are located uniformly on the image domain. Additionally, image domain has 50 mm depth and 40 mm width. Furthermore, maximum number of sensors is 128 which are located uniformly. The simulations with 128 sensors are taken as the ground truth. Then their results are compared with randomly located less sensors. MSE errors and SSIM errors can be seen from Figure 4 and 5.

In the first case, broadband excitation signal is used. Broadband excitation signal consist of 5, 7.5 and 10 MHz frequencies. Simulation results for different sensor numbers can be seen from Figure 6, 7, 8 and 9.

In the second case, narrow-band excitation signal is used for decreased range limit. 16 point scatters are placed uniformly between depth 20 mm and 35 mm. Simulation results for different sensor numbers can be seen from Figure 10, 11, 12 and 13.

In the third case, narrow-band excitation is used for regular range limit. 16 point scatters are placed uniformly between depth 10 mm and 40 mm. Simulation results for different sensor numbers can be seen from Figure 14, 15, 16 and 17.

In the fourth case, principled sampling is used rather than random sampling. One of the common approach to under sample sensor elements is to use a few terminal elements and some elements at the center. The narrow-band excitation signal is used for this scenario. Simulation results for different sensor numbers can be seen from Figure 18, 19, 20 and 21.

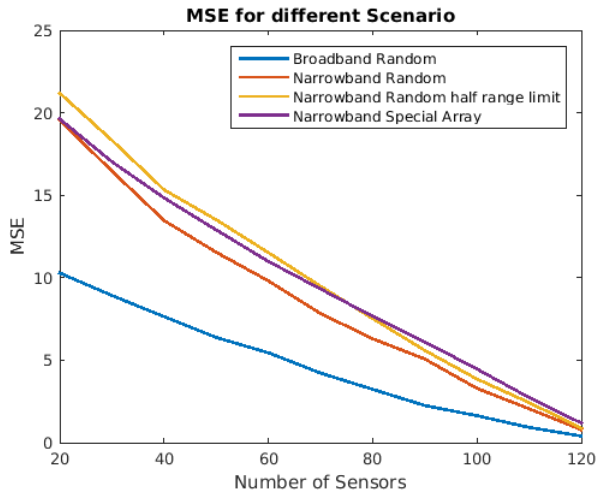

Figure 4: MSE

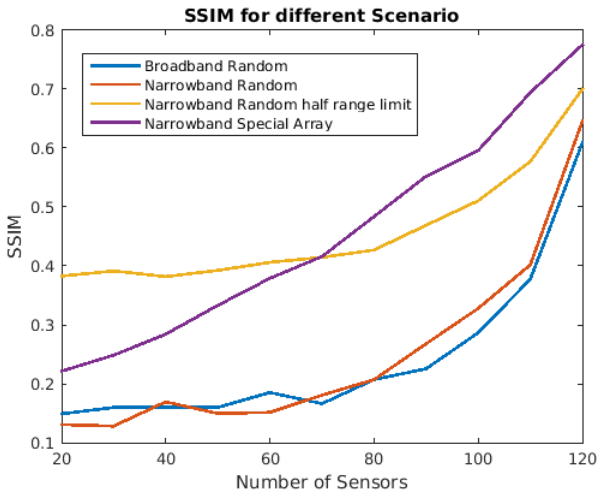

Figure 5: SSIM

In this part, the connection between simulations and problem 4 and 3 will be established. Field II simulation program can be seen as the mapping between target scene and measurements. Therefore, Field II is equivalent to matrix A.

$$FieldII : \{\text{Target scenes}\} \rightarrow \{\text{Measurements}\} \implies A : x \in \mathbb{R}^N \rightarrow y \in \mathbb{C}^{MK}$$

operator A is Field 2. Solutions to problem 4 and 3 are calculated by using beam-forming(DAS). DAS stands for delay and sum. Beam-forming is a good approximation for pseudo inverse of matrix A, i.e Beamforming $\approx A^\dagger$. So the solutions to problem 3 and 4 can be approximated as follows:

$$x_{MNLS} = A^\dagger y = A^\dagger A x_0 \implies x_{MNLS} = \text{Beamforming}\{y\} = \text{Beamforming}\{\text{Field II } \{x_0\}\}$$

Note that ΦA can be implemented by randomly eliminating sensors measurements from y. the last to be mentioned is that beam-forming operation is actually adjoint operator for A, i.e. Beamforming $\approx A^\star$. Remember that $A^\dagger = (A^\star A)^{-1} A^\star$. For a well designed systems correction factor $(A^\star A)^{-1}$ is very close to identity operator. That is why beamforming is very good approximate for pseudo inverse of A.

5 Conclusion

There are many observations. Firstly, in the paper, they are investigating single transmission multiple receiver case. In Field II simulations, multiple transmitting and multiple receiver is studied to make simulation more realistic. However, rigorous analysis of multiple transmission case is heavy. For future work, this could be a potential work. Second observation is that beamforming is very good approximate for operator A. However, rigorous calculation of pseudo-inverse of A for ultrasound imaging can be also another future research topic. Third observation is that analysis with point sources is investigated in the paper. In ultrasound there are width of each sensor element that makes analysis harder. This issue is another point to recognize. The last observations, far field assumption in the paper is a reasonable assumption for ultrasound imaging and also range limit assumption is natural since human body, which is the target scene in the ultrasound imaging, is range limited. Regarding the results from Figure 4 and 5, broadband excitation provides advantage when we consider MSE as our quantitative metric. On the other hand, principled sampling and range limit provide advantage when we consider SSIM as our quantitative measure.

References

[1] R. S. Srinivasa, M. A. Davenport, and J. Romberg, "Trading beams for bandwidth: Imaging with randomized beamforming," Jan 2019.

[2] T. L. Szabo, *Diagnostic Ultrasound Imaging: Inside Out*. Academic Press, 2014.

[3] "Statement of clinical safety regarding the use of diagnostic ultrasound." `http://sonoexams.com/physics/bioeffects/statement-of-clinical-safet.htm`. Accessed: 2019-04-01.

[4] "New "ultrasound on a chip" tool could revolutionize medical imaging." `https://spectrum.ieee.org/the-human-os/biomedical/imaging/new-ultrasound-on-a-chip-tool-could-revolu` Accessed: 2019-04-01.

[5] D. P. Woodruff, *Sketching as a Tool for Numerical Linear Algebra*. IBM Research, 2015.

[6] D. Slepian, "On bandwidth," *IEEE*, vol. 64, no. 3, pp. 292–300, 1976.

[7] Z. Zhu, S. Karnik, M. A. Davenport, J. Romberg, and M. B. Wakin, "The eigenvalue distribution of discrete periodic time-frequency limiting operators," *IEEE Signal Processing Letters*, vol. 25, no. 1, pp. 95–99, 2018.

[8] Y. Bresler, S. Basu, and C. Couvreur, *Hilbert Spaces an Least Squares Methods for Signal Processing*. 2017.

[9] J. A. Jensen, "Field: A program for simulating ultrasound systems," in *10TH NORDICBALTIC CONFERENCE ON BIOMEDICAL IMAGING, VOL. 4, SUPPLEMENT 1, PART 1:351–353*, pp. 351–353, 1996.

[10] J. A. Jensen and N. B. Svendsen, "Calculation of pressure fields from arbitrarily shaped, apodized, and excited ultrasound transducers," *IEEE transactions on ultrasonics, ferroelectrics, and frequency control*, vol. 39, no. 2, pp. 262–267, 1992.

6 Appendix

6.1 Matlab Code

```
clear all;close all;clc;
%path(path,'/home/ufuk/Desktop/UltrasoundDL/Field_II_ver_3_22_linux/');
% field_init
%% Random microbubles & Field II simulation
% Initializing the binary mask

number_elements = 100;
% disp(number_elements);
% mask = zeros(1,128);
% perm=randperm(128);
% sensorlocations = perm(1:number_elements);
% mask(sensorlocations)=1;

%initializing the Field 2 Simulation parameters
f0 = 5e6; % Transducer center frequency [Hz]
fs = 100e6; % Sampling frequency [Hz]
c = 1540; % Speed of sound [m/s]
lambda = c/f0; % Wave length [m]
width =  0.27/1000; % Width of element
element_height = 5/1000; % Height of element [m]
kerf = 0.03/1000; % Kerf [m]
focus=[0 0 20]/1000; % Fixed focal point [m]
N_elements = 128; % Number of elements in the transducer
N_active = N_elements; % Active elements in the transducer

set_sampling(fs);
emit_aperture = xdc_linear_array (N_active, width, element_height, kerf, 10, 10,
    focus);
impulse_response1 = sin(2*pi*f0*(0:1/fs:2/f0));
impulse_response2 = sin(2*pi*(7.5*f0/5)*(0:1/fs:2/f0));
impulse_response3 = sin(2*pi*(10*f0/5)*(0:1/fs:2/f0));
impulse_response = impulse_response1;% + impulse_response2 + impulse_response3;
%t = 0:1/fs:2/(f0);
%impulse_response = gauspuls(t,f0);
impulse_response = impulse_response.*hann(max(size(impulse_response)))';
xdc_impulse(emit_aperture, impulse_response);
excitation = sin(2*pi*f0*(0:1/fs:1/(f0)));
excitation = zeros(length(excitation),1)';
excitation(9)=1;
xdc_excitation(emit_aperture, excitation);
receive_aperture = xdc_linear_array(N_active, width, element_height, kerf, 10, 10,
    focus);
xdc_impulse(receive_aperture, impulse_response);
phantom_positions =
    [0/1000,0/1000,10/1000;0/1000,0/1000,20/1000;0/1000,0/1000,30/1000;...
     0/1000,0/1000,40/1000;-10/1000,0/1000,10/1000;-10/1000,0/1000,20/1000;...
     -10/1000,0/1000,3/1000;-10/1000,0/1000,40/100;10/1000,0/1000,10/1000;...
     10/1000,0/1000,20/1000;...
     10/1000,0/1000,30/1000;10/1000,0/1000,40/1000;];
phantom_amplitudes = [1;1;1;1;1;1;1;1;1;1;1;1]*1e25;
[scat,start_time] = calc_scat_all(emit_aperture,receive_aperture,phantom_positions,
    phantom_amplitudes,1);
scat = [zeros(round(start_time*fs),N_active*N_active);scat];
time_samples = size(scat);
scat = reshape(scat,[time_samples(1),N_active,N_active]);
scat = sum(scat,2);
```

```
scat = squeeze(scat);
for i=N_elements:-1:1
    if mask(i)==0
        scat(:,i)=[];
    end
end
%% DAS or Beamforming
chano = N_elements;
resol = 1*lambda;  %axial resolution
dx = resol/4; % lateral resolution
dz = resol/10;
startdepth = 0; % m
enddepth = 50e-3; %m
x = -(chano-1)/2*(width+kerf):dx:(chano-1)/2*(width+kerf); % lateral dimension of
    the FOV
z = startdepth:dz:enddepth; % axial dimension of the FOV
[X,Z] = meshgrid(x,z);
[Na,Nl] = size(X);
arrayx = (-chano/2+.5:chano/2-.5)*(width+kerf);
arrayz = zeros(1,length(arrayx));
for i=N_elements:-1:1
    if mask(i)==0
        arrayx(i)=[];
        arrayz(i)=[];
    end
end
Origin = [0,0];
Nt = 1;
X = repmat(X,[1,1,sum(mask)]);
Z = repmat(Z,[1,1,sum(mask)]);
arrayX = repmat(reshape(arrayx,[1,1,sum(mask)]),[Na,Nl,1]);% Meshgrid the array
    vector
arrayZ = repmat(reshape(arrayz,[1,1,sum(mask)]),[Na,Nl,1]);% Meshgrid the array
    vector
Steer = 0;
NoAngles = length(Steer);
N_transmit = N_elements;
N_receive = N_elements;
chano = N_receive;
Fs = fs;
twpeak = 0.50e-6;
PageEnd = size(scat,1);
 %plane wave imaging
Tx_Delay = (arrayx'- Origin(1)) * sin(Steer)/c;
Tx_Delay = Tx_Delay - min(Tx_Delay(:));

% Pixel-oriented beamforming (matrix version)
clear delay;
Tdelay = interp1(arrayx,Tx_Delay,x,'linear');
Tdelay = repmat(reshape(Tdelay,[1,Nl,1]),[Na,1,sum(mask)]); % Transmit delay
delay = round(((Z+sqrt((Z-arrayZ).^2+(X-arrayX).^2))/c+Tdelay+twpeak)*Fs);
delay(delay<=0) = 1; % clear 0 delays
delay(delay>PageEnd) = PageEnd; % clear delays beyond the sampling range
delay = sub2ind([size(scat,1),sum(mask)],delay,repmat(reshape(1:sum(mask),[1,1,sum(
    mask)]),[Na,Nl,1]));%find the indices of the data for each pixel in each channel
% Beamforming and IQ downmixing
beamformedIQ = sum(scat(delay),3);
beamformedIQ = abs(hilbert(beamformedIQ));
```

6.2 Results

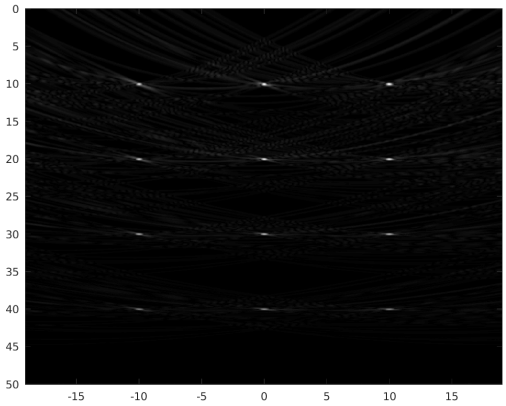

Figure 6: Broadband Excitation with 20 sensors

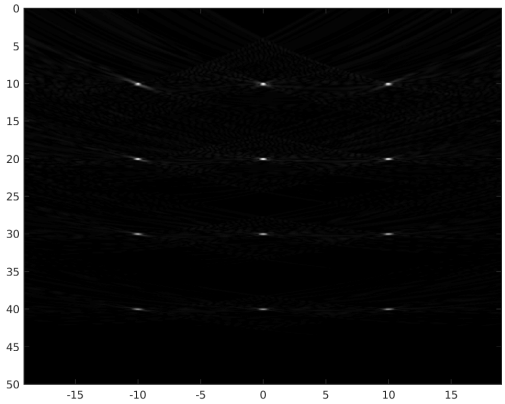

Figure 7: Broadband Excitation with 50 sensors

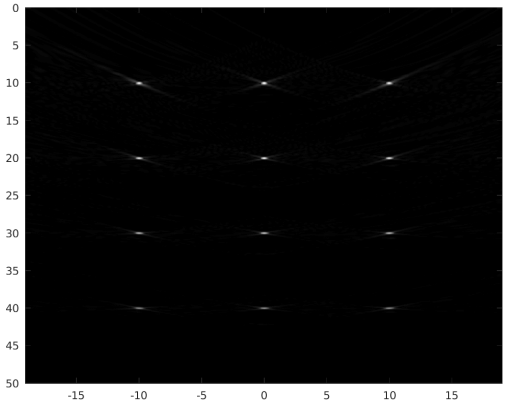

Figure 8: Broadband Excitation with 90 sensors

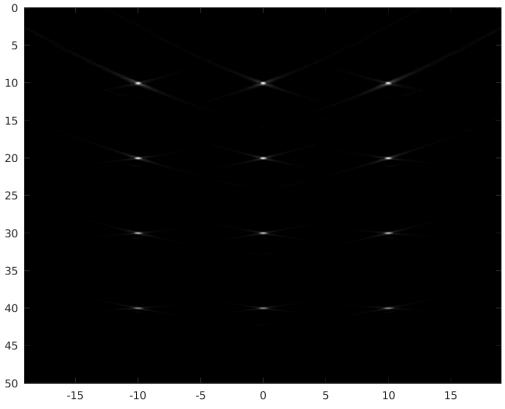

Figure 9: Broadband Excitation with 128 sensors uniformly placed(Ground Truth)

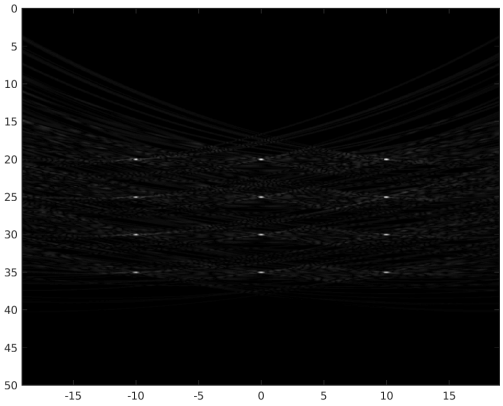

Figure 10: Narrowband Excitation with 20 sensors for decreased range-limit

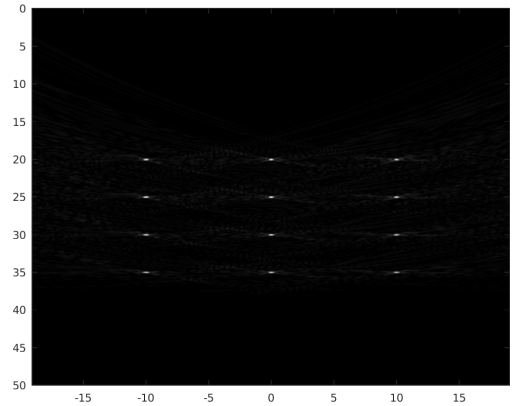

Figure 11: Narrowband Excitation with 50 sensors for decreased range-limit

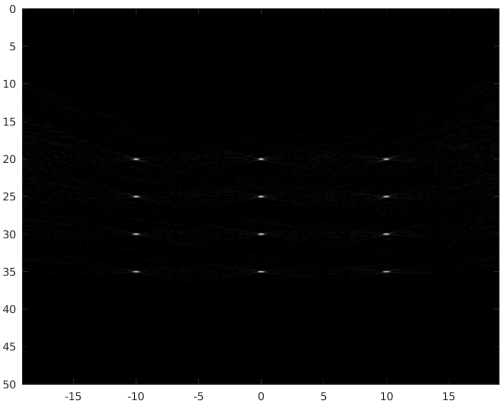

Figure 12: Narrowband Excitation with 90 sensors for decreased range-limit

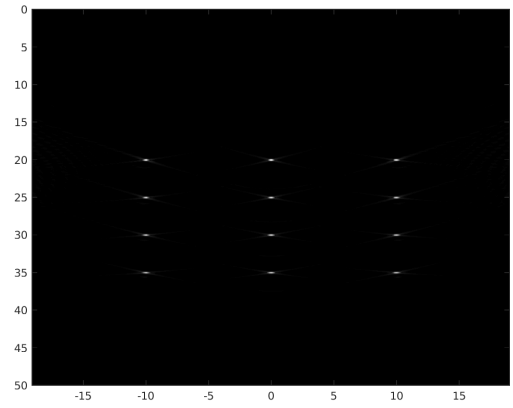

Figure 13: Narrowband Excitation with 128 sensors uniformly placed for decreased range-limit (Ground Truth)

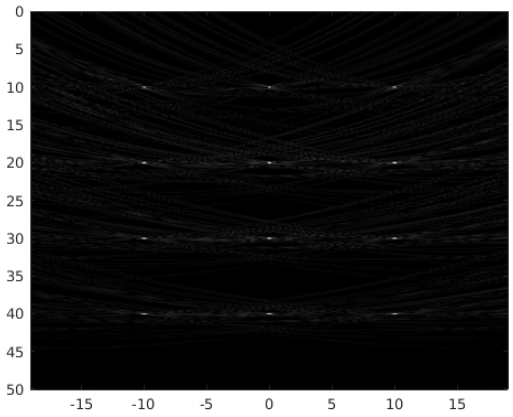

Figure 14: Narrowband Excitation with 20 sensors

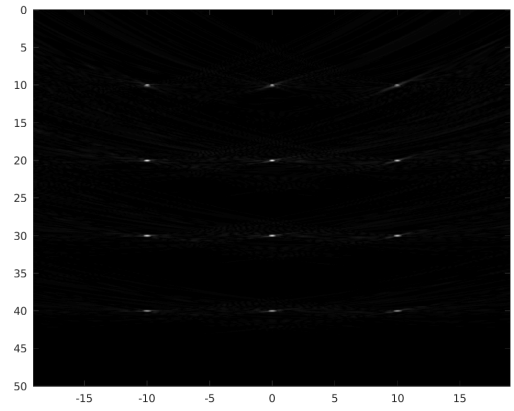

Figure 15: Narrowband Excitation with 50 sensors

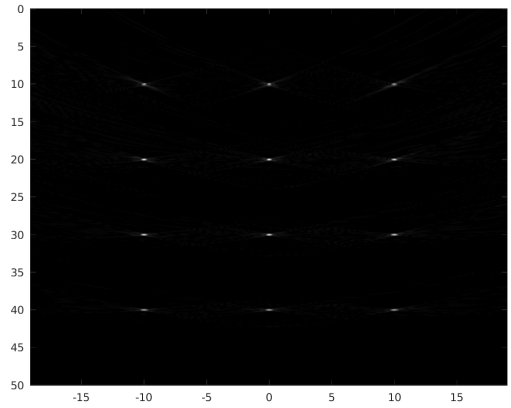

Figure 16: Narrowband Excitation with 90 sensors

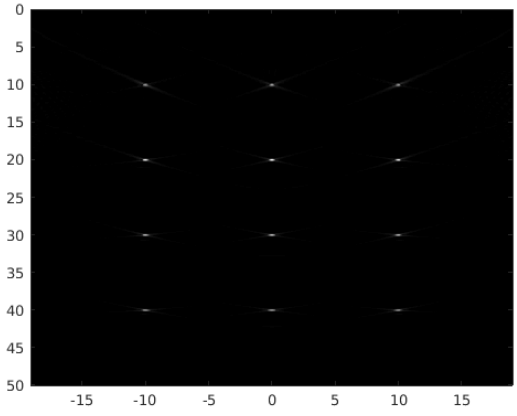

Figure 17: Narrowband Excitation with 128 sensors uniformly placed(Ground Truth)

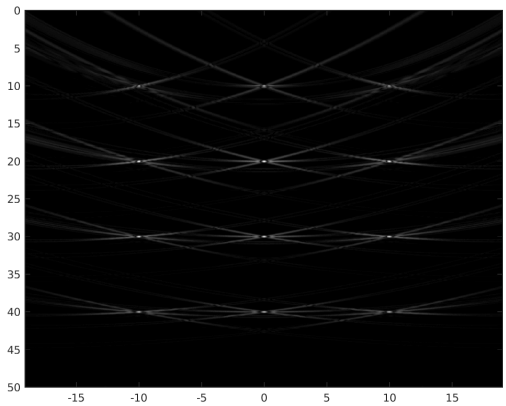

Figure 18: Narrowband Excitation with 20 sensors for principled sampling

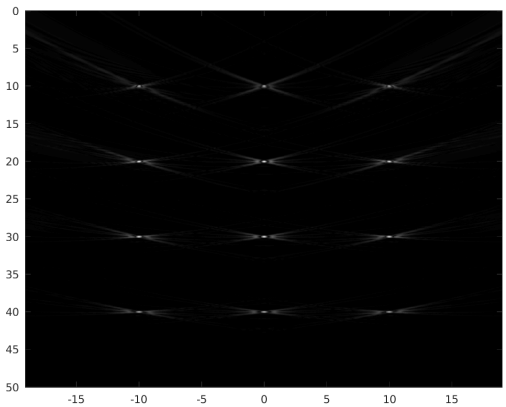

Figure 19: Narrowband Excitation with 50 sensors for principled sampling

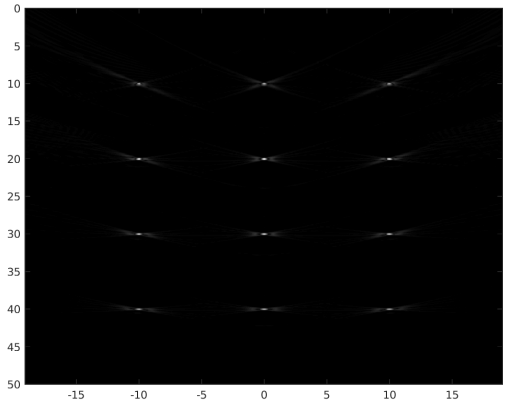

Figure 20: Narrowband Excitation with 90 sensors for principled sampling

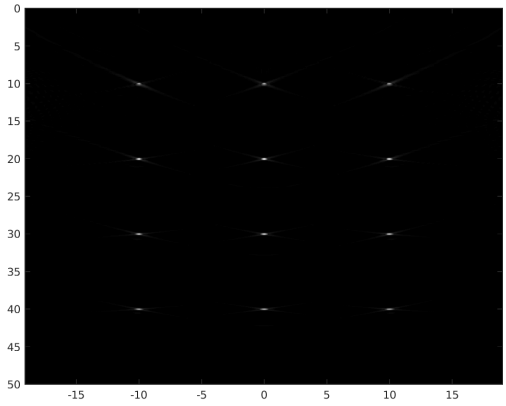

Figure 21: Narrowband Excitation with 128 sensors for principled sampling(Ground Truth)